Int J Adv Manuf Technol (2014) 71:933–941
DOI 10.1007/s00170-013-5531-7

ORIGINAL ARTICLE

A study on natural aging behavior and mechanical properties of friction stir-welded AA6061-T6 plates

H. Jamshidi Aval · S. Serajzadeh

Received: 2 June 2012 / Accepted: 29 November 2013 / Published online: 14 December 2013

Abstract Mechanical properties, microstructural events, residual stresses, and aging behavior of friction stir-welded AA6061-T6 were investigated in this work. Microstructural and mechanical characterizations of the friction stir-welded joints in as-welded and post-welded conditions were made by means of optical metallography, transmission electron microscopy, X-ray diffraction for determination of residual stresses, tensile testing, and hardness measurements. It was found that weld strength and hardness variations after welding are mainly dependent on the imposed heat input per unit length. Besides, the kinetics of natural aging in the welded samples was found to be noticeable within the first 14 days, and its effect decreases considerably in longer aging durations. The residual stress measurements show that subsequent natural aging leads to considerable relaxation of residual stress of about 22 MPa, while this effect is particularly significant in the stir zone and the thermomechanically affected zone.

Keywords Friction stir welding · 6061 aluminum alloy · Aging · Mechanical properties · Microstructural evolution

1 Introduction

As a solid-state joining technique, friction stir welding (FSW) is considered as a significant joining method in welding of similar and dissimilar aluminum alloys [1]. During this process, a weld joint is made by extrusion of thermally softened material from the leading side to the trailing side of a rotating tool, while this process is performed at much lower temperatures compared to the arc welding operations, and thus, it is possible to avoid many of the environmental and welding defects associated with arc welding operations. Accordingly, microstructural and mechanical properties of friction stir-welded materials may be affected by different factors including welding parameters, alloy composition, initial microstructures, and geometric parameters of the tool and the workpiece [1, 2]. In this regard, various investigations on friction stir welding of aluminum alloys including AA6061 were conducted to evaluate influences of welding conditions on thermal, mechanical, and microstructural responses during and/or after welding.

Mishra and Ma [3], Nandan et al. [4], and Threadgill et al. [5] have reported recent developments in process modeling, microstructure, and mechanical properties as well as the applications of friction stir welding/processing. Murr et al. [6] have studied the microstructural issues of friction stir welding of AA6061-T6, utilizing light metallography and transmission electron microscopy. Lakshminarayanan et al. [7] have compared mechanical properties of AA6061 joints fabricated by friction stir welding and arc welding techniques. Burkes et al. [8] have investigated the effects of applied load on temperature distribution, microstructure, and mechanical properties of friction stir-welded AA6061-T6. Lim et al. [9] have evaluated the effect of welding speed on mechanical properties of AA6061-T651 after FSW in which it was reported that a decreasing welding speed or an increasing rotating speed results in lower elongation of welded joints owing to the clustering of coarse Mg_2Si particles in the weld zone. Krishnan [10] has studied post-weld heat-treated friction stir-welded AA6061. The heat treatment was carried out at temperatures of 520, 540, and 560 °C followed by aging at 175 and 200 °C. It is found that the grain structures of stir zone

H. Jamshidi Aval
Department of Mechanical Engineering, Babol University of Technology, Shariati Ave., Babol, IranPO Box 484
e-mail: h.jamshidi@nit.ac.ir

S. Serajzadeh (✉)
Department of Materials Science and Engineering, Sharif University of Technology, Azadi Ave., Tehran, Iran
e-mail: serajzadeh@sharif.edu

Table 1 Welding parameter used in the experiments

Designation	Rotational speed (rpm)	Welding speed (cm/min)	Weld pitch (mm/rev)
Sample A	840	10	0.119
Sample B	840	15	0.179
Sample C	900	10	0.111
Sample D	900	15	0.167

after post-weld heat treatment (PWHT) become very coarse, and the presence of precipitate-free zones adjacent to grain boundaries leads to brittleness of the welds. Shigematsu et al. [11] have investigated the microstructural and mechanical properties of friction stir-welded 3-mm-thick AA6061 plates. İpekoğlu et al. [12] have studied the effect of temper designations on friction stir weldability of AA6061 Al–alloy plates. In the other work, the effect of post-weld heat treatment on microstructures and mechanical properties of friction stir-welded AA6061 plates was taken into account [13]. Zhang et al. [14] have studied the material flow in friction stir welding of AA6061-T6 using three-dimensional finite element modeling. Hamilton et al. [15] have predicted the thermal history and thermomechanical behavior in friction stir welding of AA6061-T6 using a three-dimensional analysis based on a finite element method. Elangovan et al. [16] have developed a mathematical model to predict a mechanical strength of friction stir-welded AA6061 by incorporating welding parameters and tool profiles. Rajesh et al. [17] have determined a temperature field during FSW of AA6061, utilizing an analytical model, and then, based on the calculated thermal history, residual stress distribution was predicted. Atharifar et al. [18] studied the material flow and heat transfer in the friction stir welding of AA6061-T6, employing a computational fluid dynamics model.

Although several works have been conducted to study the different aspects of friction stir welding of heat-treatable aluminum alloys, there is still a need for detailed studies for understanding microstructural changes and mechanical properties of this alloy after welding operations owing to subsequent natural aging. The aims of this research are to study the effects of welding parameters on mechanical and microstructural behaviors as well as residual stress distribution during and after similar joints of AA6061-T6. Accordingly, the microstructures and mechanical properties of welded alloy in as-welded and post-welded conditions are evaluated by means of hardness and tensile tests and residual stress measurements, together with optical metallography and transmission electron microcopy.

2 Experimental procedures

Friction stir welding experiments were made on the plate samples of AA6061-T6. The composition of the alloy is (in weight percent) as follows: 0.918 % Mg, 0.083 % Mn, 0.065 % Cr, 0.491 % Fe, 0.663 % Si, 0.328 % Cu, and balance Al. The aluminum plate with 5-mm thickness was cut out of the raw material. The welding samples were the first solution treated at 525 °C for 2 h and then artificially aged at 160 °C for 18 h. The artificially aged plates were then friction stir welded using rotational speeds of 840 and 900 rpm and welding speeds of 10 and 15 cm/min as listed in Table 1. As shown in Fig. 1, a FSW tool made by H13 steel with a shoulder diameter of 20 mm, 2° conical cavity, and conical probe with three grooves of 3 to 6 mm in diameter and 4.8 mm in length was used in the experiments. During welding, the inclination angle was set about 1°. Furthermore, the welded samples were allowed to be naturally aged at room temperature up to 250 days to assess the changes in mechanical properties of the weld zone after FSW. Microstructural characterization of the joints was carried out by means of an optical microscope Olympus PME3 equipped with a digital camera CLEMEX-BX51M and by transmission electron microscopy (TEM). The metallographic samples were mechanically ground and polished and then etched with a reagent made of 3 ml HNO_3,

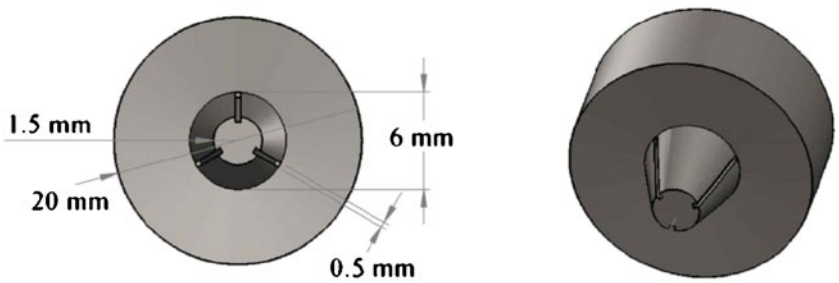

Fig. 1 The view of tool geometry used in this study

6 ml HF, 6 ml HCl, and 150 ml H_2O. Microhardness profiles were also measured across the welded joints at different locations on the transverse cross section of the joints using a Vickers indenter Peitz Wetzlar with 100 g and holding time of 15 s. The hardness measurements were performed after different aging durations for determining the changes in mechanical properties of the weld during natural aging after FSW. In order to determine the transversal and longitudinal tensile strengths of the welded samples, tensile tests were carried out. The tensile test specimens were prepared according to ASTM E8M and performed with constant crosshead speed of 1 mm/min. For the transverse tensile samples, the local strain fields were measured by digital image correlation (DIC) method using Aramis 3D 5M optical system (GOM GmbH). X-ray diffraction (XRD) technique was also utilized to measure the residual stress of the welded samples in different periods, i.e., as-welded and post-welded conditions, and longitudinal and transversal residual stress distributions were

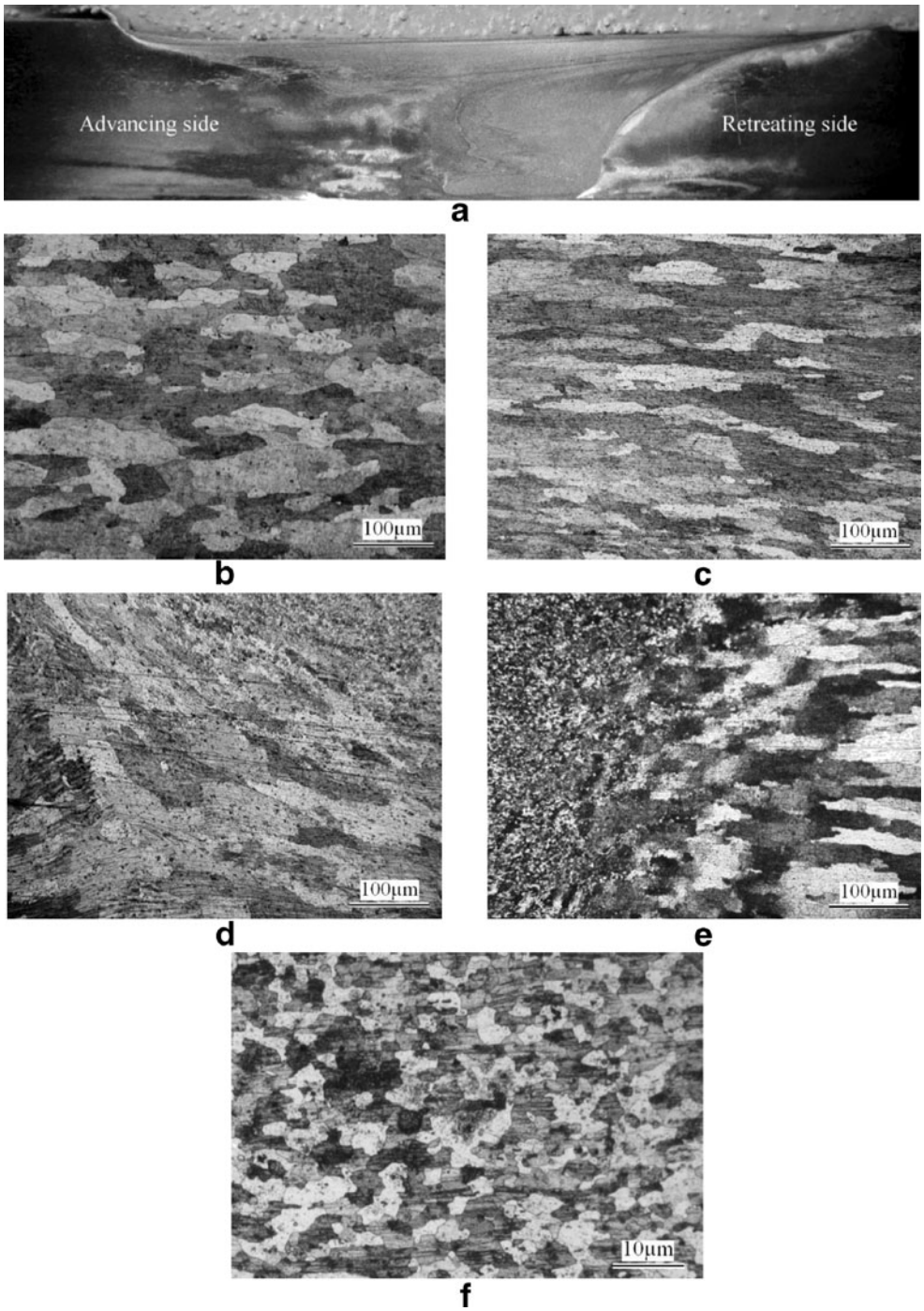

Fig. 2 Developed microstructures after FSW in sample B. **a** The view of the weld zone, **b** base material, **c** HAZ in the advancing side, **d** TMAZ in the advancing side, **e** TMAZ in the retreating side, **f** stir zone

evaluated along the direction normal to the weld line at the mid-length position of the welded plate.

3 Results and discussion

The macrostructure and three distinct microstructural zones including stir zone (SZ), thermomechanically affected zone (TMAZ), and heat-affected zone (HAZ) for sample B are shown in Fig. 2. The microstructure of the base material contains relatively large grains with the mean grain size of 65 μm as shown in Fig. 2b. As expected, the microstructure within the HAZ is somehow similar to the base material (Fig. 2c). The grains within TMAZ of the advancing side are deformed and elongated as a result of the fiber structure that formed during deformation as shown in Fig. 2d. Figure 2e also displays the microstructure of the retreating side in which no clear deformation structure such as twins and elongated grains can be detected. Moreover, the boundary between SZ and TMAZ cannot be clearly distinguished in the retreating side. As shown in Fig. 2f, microstructure of stir zone consists of fine and equiaxed grains as a result of continuous dynamic recrystallization that occurs during severe plastic deformation at high temperatures [3].

Figure 3 illustrates the horizontal hardness profiles across the joints of samples B and C measured at 2 mm from the root face, while the hardness AA6061-T6 base metal was about 101 HV. In heat-treatable alloys such as AA6061, the different

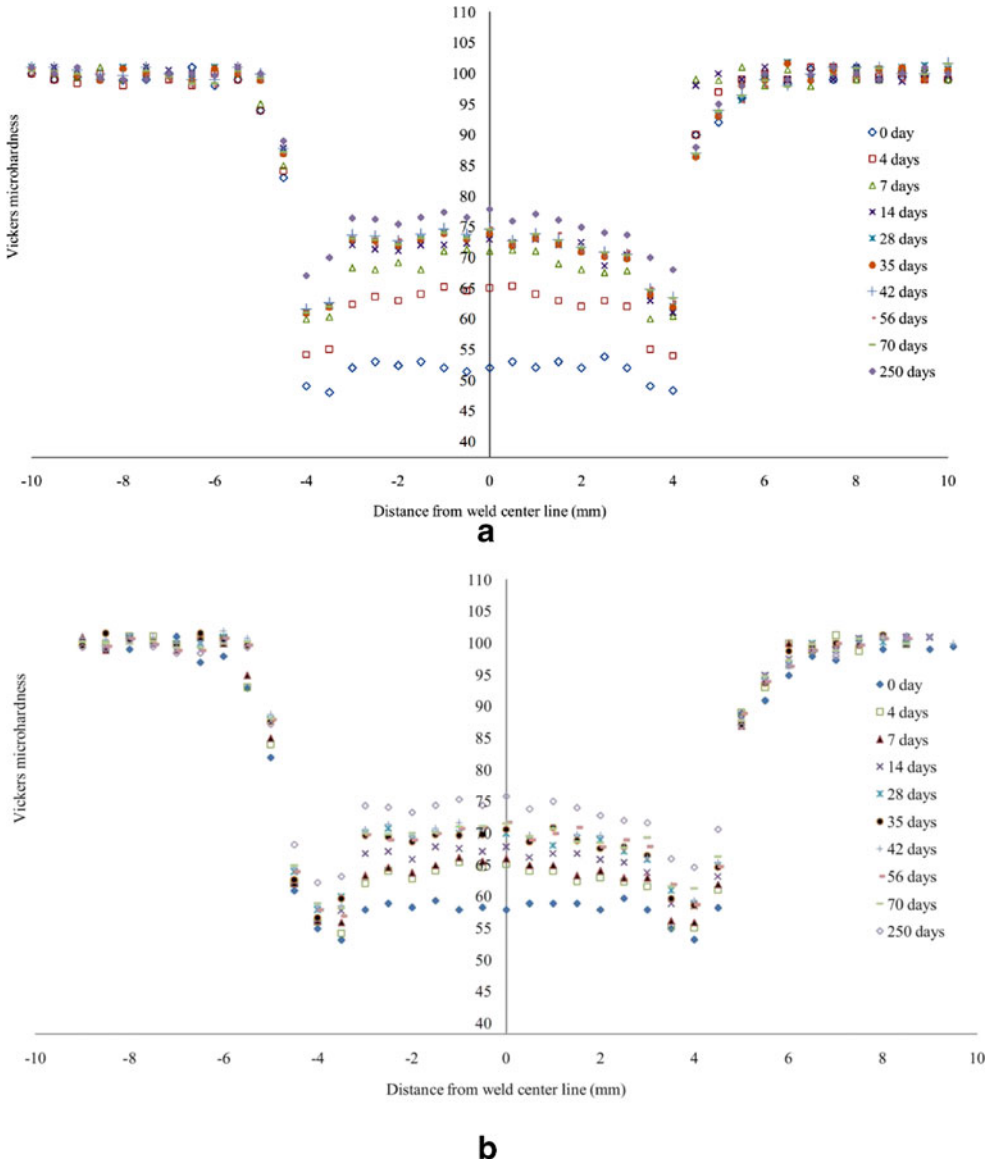

Fig. 3 Microhardness profile of samples: **a** sample B and **b** sample C

phenomena may occur in HAZ, TMAZ, as well as in the stir zone depending on the imposed heat flux, strain distribution, and cooling rate of the welded samples. Accordingly, the abovementioned regions may be left in overaged condition, partially solution-treated conditions, or single-phase solid solution. It should be noted that, in the nonequilibrium solid solution AA6061, the decomposition proceeds in the following steps: the formation of needle-like zones along the <100> Al crystal direction, the ordering of their structure and the formation of β'' needles, the transition from β'' needles to β' rods, and the formation of equilibrium β (Mg_2Si) phase [19]. The β'' precipitate has shown an effective role on strengthening the aged alloys, while the Mg_2Si precipitate has little contribution to the strengthening of AA6061. According to Fig. 3, an abrupt decrease in hardness can be observed across the joints due to partial dissolution and coarsening of the hardening particles. Similar results have reported in case of FSW of heat-treatable aluminum alloys including 6061-T6 and 7075-T6 in which the overaging can take place in HAZ [13, 20, 21]. The as-welded hardness distribution in samples B and C are almost the same; however, the weld zone is larger in sample C with higher heat input, i.e., higher rotational speed and smaller linear velocity. On the other hand, both samples show a similar trend of natural aging after 250 days in which the hardness in the stir zone reaches to about 78 HV and 74 HV in samples B and C, respectively. Note that the hardness increases rapidly in TZ and TMAZ approximately up to 14 days, while in longer aging periods, it increases with a slower rate (Fig. 4). Figure 5 also shows the TEM images of base material, TZ, TMAZ, and HAZ in sample C after 250 days of natural aging. Base material contains needle-type precipitates in the range of 21–44 nm length and Si-rich round precipitates surrounded by a web of dislocations shown in Fig. 5a. This microstructure displays a good correlation with observations in previous studies about β'' needle phase by Olea et al. [22]. As shown in Fig. 5b, the HAZ microstructure contains rod-shaped precipitates with size in the range of 65–110 nm length and 4–13 nm width together with 5–18 nm round precipitates. According to the selected area diffraction pattern (SADP) and previous study by Chakrabarti and Laughlin [23], the rod phase can be β' particles, and round precipitates are β (Mg_2Si) particles. According to TEM image of TMAZ as displayed in Fig. 5c, dissolved rod-shaped precipitates and round-shaped precipitates in a relatively wide range of 50–200 nm in size are observed. These changes in the size and morphologies of the precipitates justify the abrupt reduction of TMAZ hardness. On the other hand, Figs. 2 and 5d show that the stir zone includes a large number of rods and round phases within a fine and equiaxed grain structure resulted from dynamic recrystallization during FSW [2, 3]. It is worth stating that the increase in the hardness can be related to

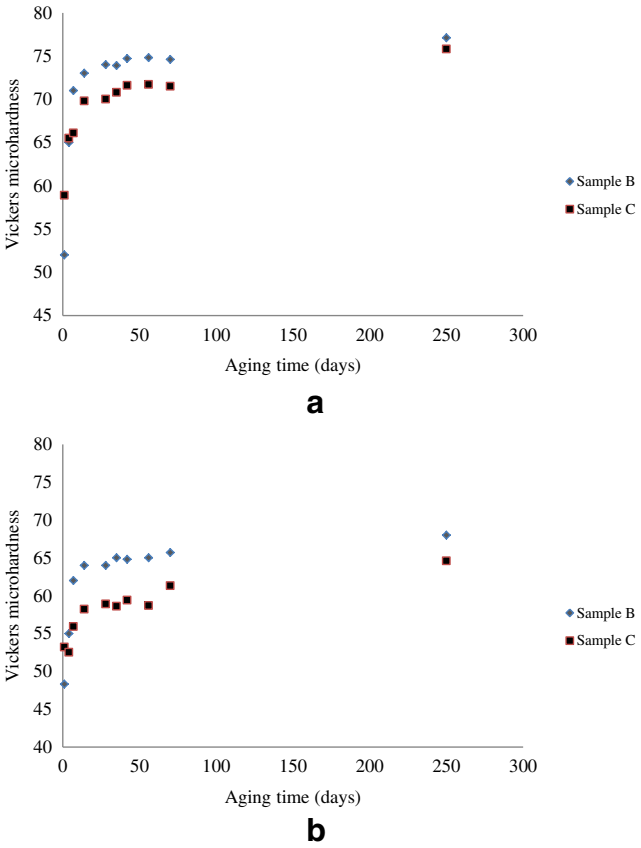

Fig. 4 Microhardness vs. aging time of samples B and C. **a** Stir zone, **b** TMAZ

the formation of GP zones and β'' precipitates during natural aging within the stir zone.

The results of the tensile tests for all samples after natural aging for periods of 7 and 70 days are shown in Fig. 6 where the yield and tensile strengths of base material, i.e., AA6061-T6, are about 278 and 315 MPa, respectively. It has been reported that heat generation (Q_t) by the shoulder is an important factor in FSW operations, and also, the final properties of the weld are strongly influenced by this factor [24]. The FSW tool moves during FSW, and thus, the heat flow during FSW should be evaluated by "Q_t/S" where S denotes welding speed. In addition, the heat generation (Q_t) is directly dependent on the tool rotational speed (ω) [24]. Therefore, the speed ratio (ω/S) could be considered as a measure of heat input per unit length of the weld. The results show that the yield stress of the welded sample is less than that of the base material, while the yield stress of welded alloys lightly decreases as the imposed heat input increases. Figure 7a compares the stress–strain diagrams of the AA6061 in T4 and T6 temper conditions with those obtained for the stir zone of sample C in as-welded and naturally aged conditions. It is seen that the initial strength, i.e., T6 condition, is never reached during

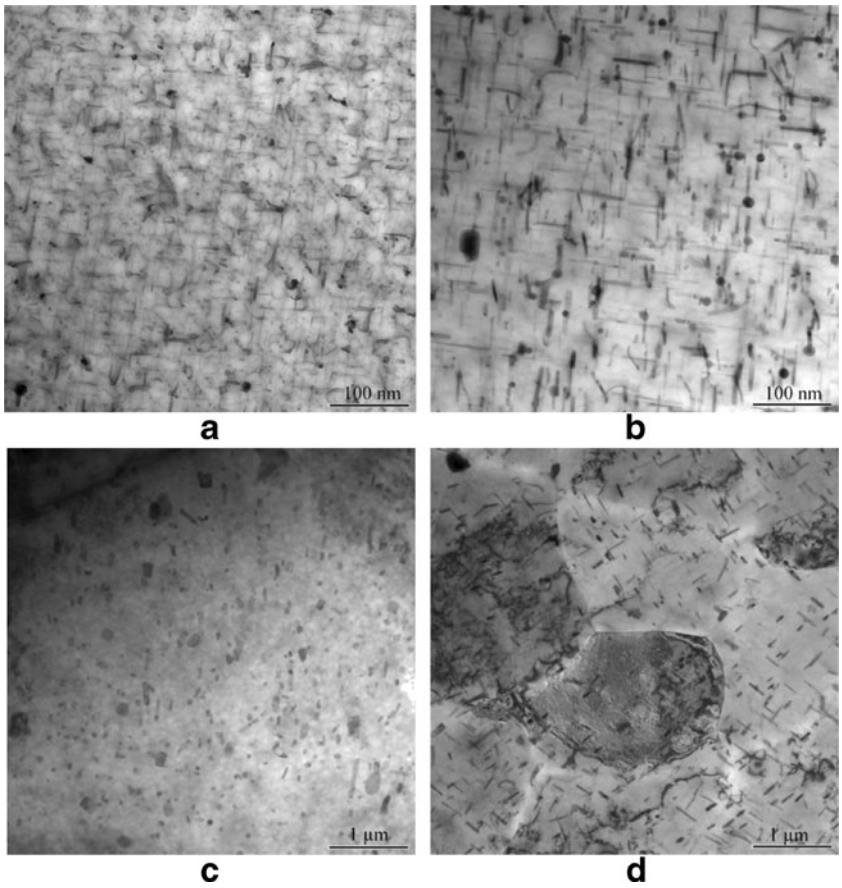

Fig. 5 TEM images taken from sample C. **a** Base metal, **b** HAZ, **c** TMAZ, **d** stir zone

subsequent natural aging; however, the tensile stress of naturally aged welds is obviously higher than that for the AA6061-T4 condition. It may be attributed to the effect of grain refinement in the weld nugget that enhances the nucleation rate, and thus, it produces a fine and dispersed distribution of strengthening precipitates. It is interesting to note that the as-welded sample shows a serrated flow, while this effect is disappeared after aging for 7 days. The possible reason of serrated flow can be attributed to immobilizing of dislocations by in-solution substitutional atoms during tensile test [25]. Note that in welding stage, partial solution treatment takes place that produces a supersaturated substitutional solid solution. As a result, the Portevin–Le Chatelier (PLC) effect is expected to be operative in as-welded material; however, after a certain aging duration, i.e., after about 7 days for the conditions employed in this work, substitutional atoms like Mg atom take part in precipitation process, and therefore, PLC serrations disappeared due to the formation of new strengthening particles. Figure 7b shows the strain maps and the local tensile properties of different weld subzones in sample C. As shown in this figure, fracture in the tensile sample occurs in the TMAZ of the advancing side, where a sudden change in hardness is observed according to Fig. 3. The local stress–strain curves were computed from local strain field achieved by DIC method based on a method explained in the study of Leitão et al. [26]. Comparing strain map and hardness profile shows a rational consistency between DIC data and hardness

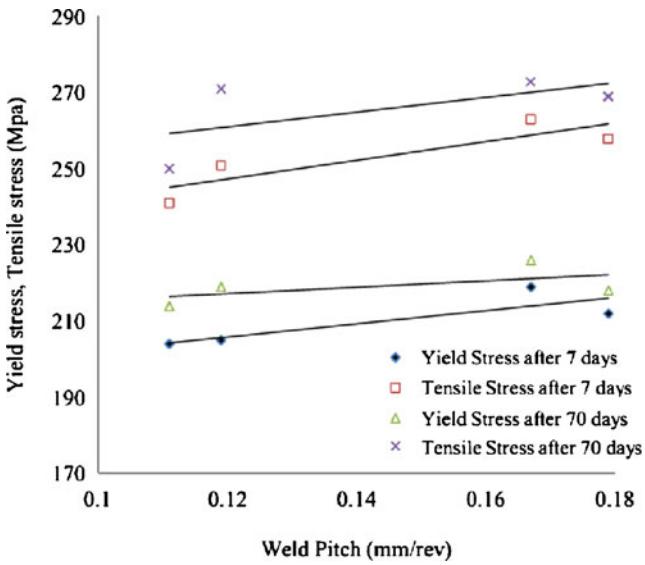

Fig. 6 The relationship between mechanical properties of FS-welded samples and heat input

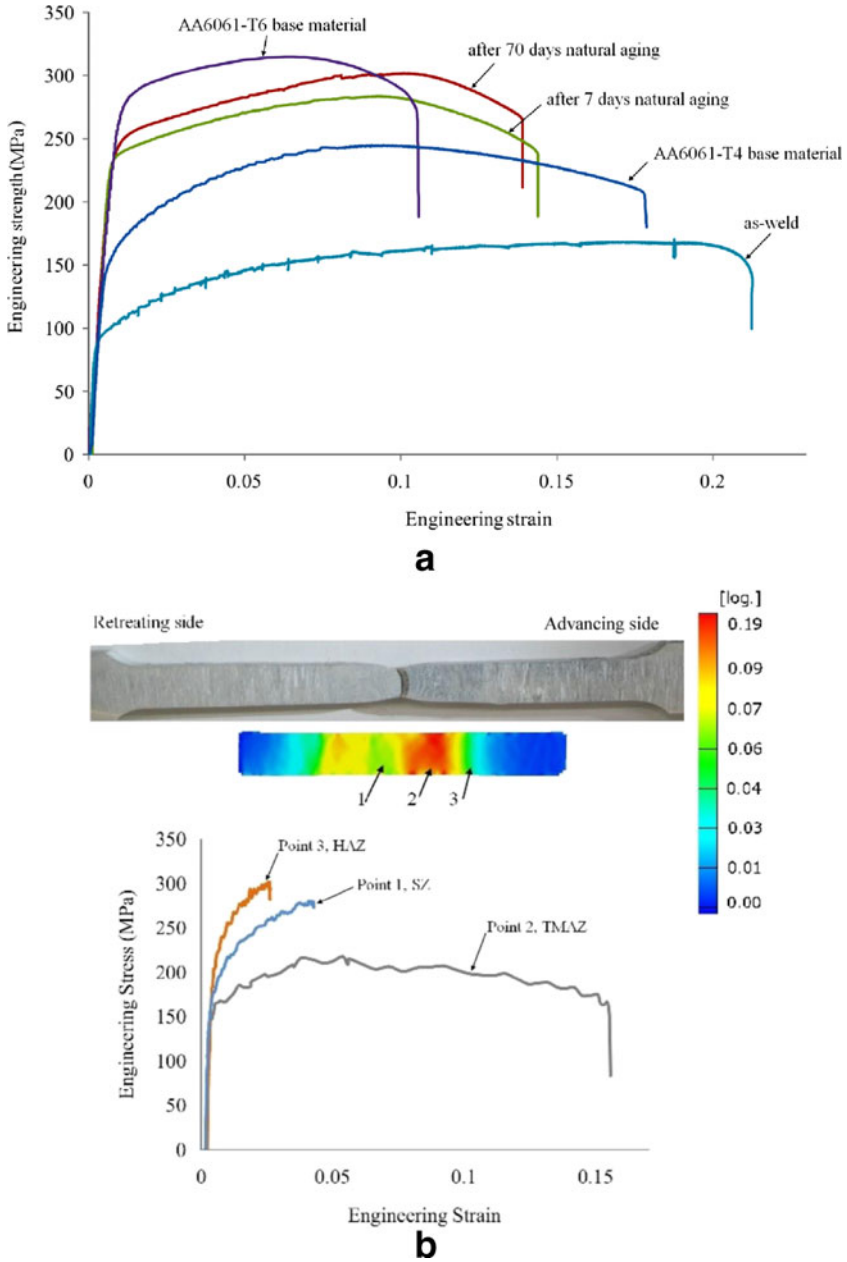

Fig. 7 **a** Stress–strain diagrams of AA6061-T6, AA6061-T4, and sample C. **b** The strain maps and the local mechanical properties of different weld subzones for sample C

profile of the weldment. For instance, the yield strength and average microhardness of TMAZ in sample C are 155 MPa and 65 HV, respectively, while the yield strength and average microhardness of HAZ increase to 256 MPa and 94 HV, respectively.

Finally, Fig. 8 shows the measured longitudinal and transverse residual stress distribution in the sample C after natural aging for periods of 7 and 70 days. This figure clearly shows the changes in residual stress distributions during subsequent aging, particularly in the stir zone and the thermomechanically affected zone. As seen, the longitudinal residual stresses around the weld line are tensile and almost the same at the retreating and advancing sides, while their nature gradually changes to being compressive beyond the heat-affected zone. The tensile residual stress in the weld centerline is lower than the TZ/TMAZ interface. Similar behavior occurs in the transversal residual stress profiles with a main difference; the longitudinal residual stresses are approximately two times higher than transverse residual stresses. As stated above, the important point in Fig. 8 is that the residual stresses change as the natural aging proceeds. This indicates interconnection between aging kinetics and relaxation of residual stresses within the weld sample. In this regard, a decrease in the residual after a 70-day aging period occurs within

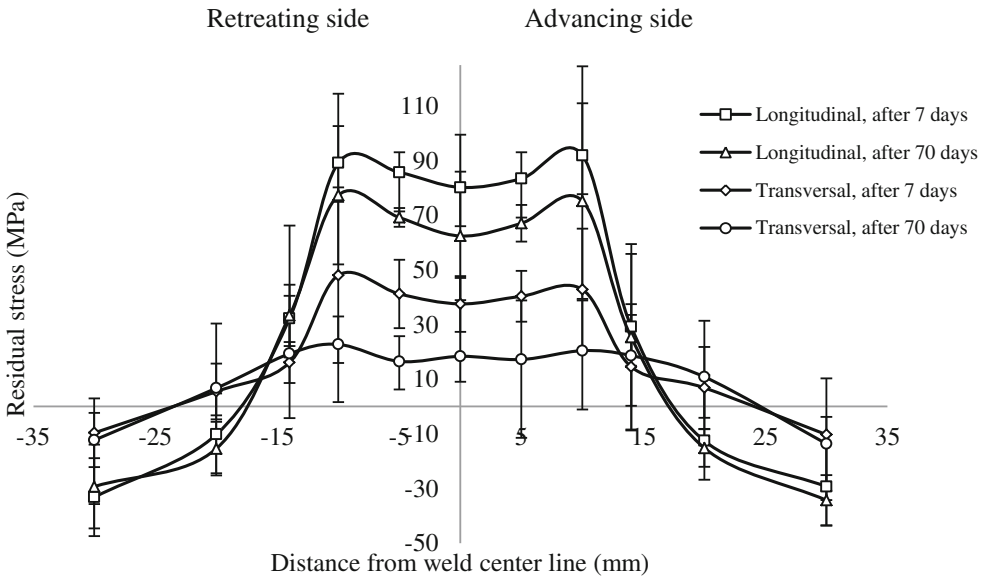

Fig. 8 Residual stress distribution vs. natural aging time for sample C

the stir zone, and considerable stress relaxation of about 22 MPa has been detected. This point is particularly important in the application of the weldment under fatigue loading. A similar influence on residual stresses during natural aging conditions has been reported by Woo et al. [27] in thermomechanically deformed materials.

4 Conclusions

In this study, aging behavior, mechanical properties, microstructures, and distribution of residual stresses after friction stir welding of AA6061-T6 have been evaluated by optical microscopy, transmission electron microscopy, tensile testing, microhardness, and X-ray residual stress measurements in as-welded and post-welded conditions. The results can be summarized as follows:

- A considerable decrease in hardness is observed across the as-welded joints due to partial dissolution and coarsening of the hardening particles.
- The natural aging in the welded samples significantly affects the mechanical properties during the first 14 days; however, its effect decreases considerably in longer aging durations.
- The longitudinal and transverse residual stress in the stir zone shows noticeable decreases during subsequent natural aging, while no significant decreases were observed in the base metal and HAZ.
- The particle morphologies in HAZ are in forms of rod and round shapes, while in the TMAZ, the rod-shaped precipitates are mostly dissolved, and the round precipitates with the diameters in the range of 50–200 nm are observed.

References

1. Thomas WM, Needham JC, Murch MG, Templesmith P, Dawes CJ (1991) Friction stir welding, international patent application no. PCT/GB92102203 and Great Britain patent application no. 9125978.8
2. Çam G (2011) Friction stir welded structural materials: beyond Al-alloys. Int Mater Rev 56:1–48
3. Mishra RS, Ma ZY (2005) Friction stir welding and processing. Mater Sci Eng R 50:1–78
4. Nandan R, DebRoy T, Bhadeshia HKDH (2008) Recent advances in friction-stir welding—process, weldment structure and properties. Prog Mater Sci 53:980–1023
5. Threadgill PL, Leonard AJ, Shercliff HR, Withers PJ (2009) Friction stir welding of aluminium alloys. Int Mater Rev 54:49–93
6. Murr LE, Liu G, Mcclure JC (1998) A TEM study of precipitation and related microstructures in friction-stir-welded 6061 aluminium. J Mater Sci 33:1243–51
7. Lakshminarayanan AK, Balasubramanian V, Elangovan K (2009) Effect of welding processes on tensile properties of AA6061 aluminium alloy joints. Int J Adv Manuf Technol 40:286–296
8. Burkes DE, Hallinan NP, Shropshire KL, Wells PB (2008) Effects of applied load on 6061-T6 aluminum joined employing a novel friction bonding process. Metall Mater Trans A 39:2852–2861
9. Lim S, Kim S, Lee CG, Kim S (2004) Tensile behavior of friction-stir-welded Al 6061-T651. Metall Mater Trans A 35:2829–2835
10. Krishnan KN (2002) The effect of post weld heat treatment on the properties of 6061 friction stir welded joints. J Mater Sci 37:473–480
11. Shigematsu I, Kwon YJ, Suzuki K, Imai T, Saito N (2003) Joining of 5083 and 6061 aluminum alloys by friction stir welding. J Mater Sci Lett 22:353–356
12. İpekoğlu G, Erim S, Gören Kıral B, Çam G (2013) Investigation into the effect of temper condition on friction stir weldability of AA6061 Al-alloy plates. Kovove Mater 51:155–163
13. İpekoğlu G, Erim S, Çam G (2013) Investigation into the influence of post-weld heat treatment on the friction stir welded AA6061 Al-alloy

plates with different temper conditions. Metall Mater Trans A. doi:10.1007/s11661-013-2026-y
14. Zhang HW, Zhang Z, Chen JT (2007) 3D modeling of material flow in friction stir welding under different process parameters. J Mater Process Technol 183:62–70
15. Hamilton C, Dymek S, Sommers A (2008) A thermal model of friction stir welding in aluminum alloys. Int J Mach Tools Manuf 48:1120–1130
16. Elangovan K, Balasubramanian V, Babu S (2009) Predicting tensile strength of friction stir welded AA6061 aluminium alloy joints by a mathematical model. Mater Des 30:188–193
17. Rajesh SR, Bang HS, Chang WS, Kim HJ, Bang HS, Oh CI, Chu JS (2007) Numerical determination of residual stress in friction stir weld using 3D-analytical model of stir zone. J Mater Process Technol 187–188:224–226
18. Atharifar H, Lin D, Kovacevic R (2009) Numerical and experimental investigations on the loads carried by the tool during friction stir welding. J Mater Eng Perform 18:339–350
19. Totten GE, MacKenzie DS (eds) (2003) Handbook of aluminum; physical metallurgy and processes, vol 1. Marcel Dekker Inc, New York
20. İpekoğlu G, Gören Kıral B, Erim S, Çam G (2012) Investigation of the effect of temper condition on friction stir weldability of AA7075 Al-alloy plates. Mater Technol 46:627–632
21. İpekoğlu G, Erim S, Çam G (2013) Effects of temper condition and post weld heat treatment on the microstructure and mechanical properties of friction stir butt welded AA7075 Al-alloy plates. Int J Adv Manuf Technol. doi:10.1007/s00170-013-5255-8
22. Olea CA, Roldo L, dos Santos JF, Strohaecker TR (2007) A substructural analysis of friction stir welded joints in an AA6056 Al-alloy in T4 and T6 temper conditions. Mater Sci Eng A 454–455:52–62
23. Chakrabarti DJ, Laughlin DE (2004) Phase relations and precipitation in Al–Mg–Si alloys with Cu additions. Prog Mater Sci 49:389–410
24. Schmidt H, Hattel J, Wer J (2004) An analytical model for the heat generation in friction stir welding. Model Simul Mat Sci Eng 12:143–57
25. Hall EO (1970) Yield point phenomena in metals and alloys. Plenum Press, New York
26. Leitão IGC, Leal RM, Rodrigues DM (2012) Determination of local constitutive properties of aluminium friction stir welds using digital image correlation. Mater Des 33:69–74
27. Woo W, Feng Z, Wang XL, Hubbard CR (2009) Neutron diffraction measurements of time-dependent residual stresses generated by severe thermo-mechanical deformation. Scr Mater 61:624–7